Intensity squeezing in a Raman laser

A. Eschmann and R. J. Ballagh
Physics Department, University of Otago, Dunedin, New Zealand
(Received 30 June 1998)

Quantum noise suppression in a Raman laser is investigated theoretically using a model system of homogeneously broadened three-state atoms, driven by an external pump field. Arbitrary pump, Raman, and cavity detunings are allowed, and the full dynamical response of the system is included in the treatment of quantum noise. The behavior of the intensity squeezing of both the pump and Raman fields is reported for a wide parameter regime in which optically bistable switching occurs. [S1050-2947(99)03407-1]

PACS number(s): 42.55.Ye, 42.50.Dv, 42.50.Lc

I. INTRODUCTION

The phenomenon of Raman lasing has attracted a great deal of theoretical and experimental study. Much of this work has been concerned with the deterministic behavior of the system, such as fundamental mechanisms of Raman gain (e.g., Refs. [1–3]), or the nonlinear dynamical and switching behavior [4–8]. Studies of specifically quantum-mechanical properties of the Raman field are fewer and have concentrated mainly on the description of initiation, and the analysis of the large-scale fluctuations observed in the build up of Stokes pulses (e.g., Refs. [9–12]). The possibility of quantum noise suppression (or squeezing) has only recently been recognized and a number of calculations have been made [13–18] which show that the statistics of the Raman field may deviate from Poissonian. However, in all of those treatments the models used are quite limited, and in this paper we make significant extensions to the models and find this leads to enhanced regimes and quality of squeezing.

In the previous treatments of Raman squeezing, the pump laser field is treated as a prescribed classical field, and the atomic dynamics are adiabatically eliminated by assumption of the good cavity limit. However, the Raman laser is a complex dynamical system, and the states of the intracavity pump and Raman fields, including the Raman frequency, are dynamically determined by an interplay between fields and atoms. Of the previous treatments, only Schernthanner and Ritsch [18] allow for the possibility of detunings between fields, atoms, and cavity, but they ignore the dynamical nature of the Raman frequency and make it a prescribed value. In the current paper, we retain the atomic dynamics, and fully incorporate the effect of the field detunings. The issue of detunings is an important one; for example, the switching and nonlinear dynamical behavior previously observed in Raman lasers [7–19] depend critically on the detunings between fields, cavity resonances, and atomic transitions. Our results show that squeezing occurs primarily in the regimes where switching occurs, as could perhaps have been anticipated, since it is here that the effects of system nonlinearity are greatest.

As in the previous treatments of squeezing [13–18], our model consists of a collection of homogeneously broadened three-state atoms in the λ configuration, but we allow the pump field to be detuned both from its atomic transition and the vacuum cavity resonance. The (vacuum) cavity resonance for the Raman field is also an adjustable parameter of the theory, but the Raman frequency is a system variable that is determined by the system behavior. We employ a master equation treatment which describes the full dynamical response of the atomic system, and includes the quantum noise in a comprehensive manner. The complexities of the model are sufficient that the standard techniques [20,21] for converting the master equation to quantum stochastic differential equations must be replaced by the more general phase-space methods of Smith and Gardiner [22], and numerical methods are required to find the squeezing behavior. We carry out an extensive investigation of the squeezing that can occur in the transmitted pump field and the Raman field, and give a systematic summary of the squeezing behavior within the regimes of switching and its dependence on system parameters. Previous papers have concentrated on calculating the Mandel Q parameter, and in those papers where the squeezing spectrum was considered, since the adiabatic limit is assumed, the eigenvalues of the drift matrix were taken to always be real, yielding Lorentzian spectra. We calculate the squeezing spectrum directly, and find that it can be far from Lorentzian.

The paper is organized as follows. A detailed description of the system is given in Sec. II, and the master equation is obtained from the Hamiltonian. In Sec. III, we derive the Fokker-Planck equation for fields and atoms using the method of Smith and Gardiner, and the quantum stochastic differential equations (QSDEs) are then written down in an appropriately scaled form. A method for solving for the steady-state system behavior is outlined in Sec. IV, and in Sec. V the stochastic equations are linearized. Some broad categories of possible steady-state deterministic behavior and the dependence on system parameters are discussed in Sec. VI. In Sec. VII, the squeezing calculation is outlined, and in Sec. VIII results are presented.

II. DESCRIPTION OF THE SYSTEM

The atomic system is modeled as a collection of N stationary three-state atoms in the λ configuration [19,25]. The various processes occurring between the three states are displayed in Fig. 1. We allow for detunings between the pump (at frequency ω_p) and Raman (at frequency ω_r) fields and their corresponding atomic transition [$\Delta = \omega_p - (\omega_3 - \omega_1) = \omega_p - \omega_{31}$ and $\Delta_r = \omega_r - (\omega_3 - \omega_2) = \omega_r - \omega_{32}$, respec-

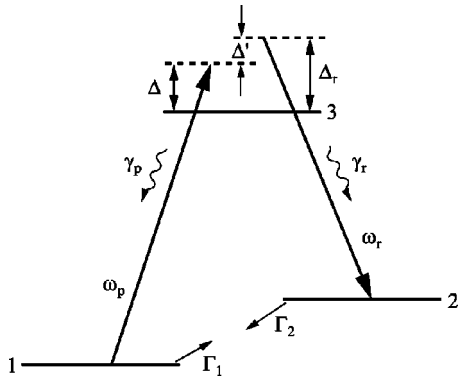

FIG. 1. The three-state atom model showing detunings and population transfer rates (in scaled units).

tively]. $\overline{\Delta}' = \overline{\Delta}_r - \overline{\Delta}$ is the detuning from exact two-photon resonance. All quantities are initially introduced in S.I. units, but will subsequently be rescaled into dimensionless units. For clarity, those quantities which later appear in dimensionless form are indicated here with a bar. The Hamiltonian for the system can be written as a sum of free contributions (H_F), interaction contributions (H_I), and decay contributions (H_D), in the electric dipole and rotating wave approximations:

$$H = H_F + H_I + H_D, \tag{1}$$

where

$$H_F = H_{PF} + H_{RF} + H_{AF}, \tag{2}$$

$$H_I = H_{AP} + H_{AR} + H_{EP}, \tag{3}$$

$$H_D = H_{PD} + H_{RD} + H_{A_1D} + H_{A_2D} + H_{A_3D}, \tag{4}$$

and

$$H_{PF} = \hbar \omega_p^c \hat{p}^\dagger \hat{p}, \tag{5}$$

$$H_{RF} = \hbar \omega_r^c \hat{r}^\dagger \hat{r}, \tag{6}$$

$$H_{AF} = \sum_{\mu=1}^{N} (\hbar \omega_1 \hat{\sigma}_{11}^\mu + \hbar \omega_2 \hat{\sigma}_{22}^\mu + \hbar \omega_3 \hat{\sigma}_{33}^\mu), \tag{7}$$

$$H_{AP} = \sum_{\mu=1}^{N} i\hbar (\overline{g}_p \hat{\sigma}_{13}^\mu \hat{p}^\dagger - \overline{g}_p^* \hat{\sigma}_{13}^{\dagger\mu} \hat{p}), \tag{8}$$

$$H_{AR} = \sum_{\mu=1}^{N} i\hbar (\overline{g}_r \hat{\sigma}_{23}^\mu \hat{r}^\dagger - \overline{g}_r^* \hat{\sigma}_{23}^{\dagger\mu} \hat{r}), \tag{9}$$

$$H_{EP} = i\hbar (\hat{p}^\dagger \overline{\varepsilon} e^{-i\omega_p t} - \hat{p} \overline{\varepsilon}^* e^{i\omega_p t}), \tag{10}$$

$$H_{PD} = (\hat{p}^\dagger \hat{\xi}_p + \hat{p} \hat{\xi}_p^\dagger), \tag{11}$$

$$H_{RD} = (\hat{r}^\dagger \hat{\xi}_r + \hat{r} \hat{\xi}_r^\dagger), \tag{12}$$

$$H_{A_1D} = \sum_{\mu=1}^{N} (\hat{\sigma}_{13}^{\dagger\mu} \hat{\Xi}_p + \hat{\sigma}_{13}^\mu \hat{\Xi}_p^\dagger + \hat{\sigma}_{23}^{\dagger\mu} \hat{\Xi}_r + \hat{\sigma}_{23}^\mu \hat{\Xi}_r^\dagger), \tag{13}$$

$$H_{A_2D} = \sum_{\mu=1}^{N} (\hat{\sigma}_{33}^\mu \hat{\zeta}_3 + \hat{\sigma}_{22}^\mu \hat{\zeta}_2 + \hat{\sigma}_{11}^\mu \hat{\zeta}_1 + \hat{\zeta}_3^\dagger \hat{\sigma}_{33}^\mu + \hat{\zeta}_2^\dagger \hat{\sigma}_{22} + \hat{\zeta}_1^\dagger \hat{\sigma}_{11}^\mu), \tag{14}$$

$$H_{A_3D} = \sum_{\mu=1}^{N} (\hat{\eta}_2^\dagger \hat{\sigma}_{12}^\mu + \hat{\sigma}_{12}^{\dagger\mu} \hat{\eta}_2 + \hat{\eta}_1 \hat{\sigma}_{12}^{\dagger\mu} + \hat{\sigma}_{12}^\mu \hat{\eta}_1^\dagger). \tag{15}$$

The various contributions to the Hamiltonian have the following meanings.

(i) H_{PF} is the free Hamiltonian for the pump cavity field mode, where ω_p^c is the empty-cavity resonant frequency closest to the actual pump frequency ω_p, and $\hat{p}$ is the destruction operator for the pump photon.

(ii) H_{RF} is the free Hamiltonian for the Raman cavity field mode, where ω_r^c is the empty-cavity resonant frequency closest to the Raman frequency ω_r and $\hat{r}$ is the destruction operator for the Raman photon. We note that ω_r is not a predetermined frequency, but instead is determined by the operating conditions of the system.

(iii) H_{AF} is the free Hamiltonian for the atoms. The energies of the three atomic states are $\hbar\omega_1$, $\hbar\omega_2$, and $\hbar\omega_3$.

(iv) H_{AP} and H_{AR} describe the dipole coupling of the atoms to the pump and Raman fields, respectively, where $\overline{g}_p$ and $\overline{g}_r$ are the dipole coupling constants for the $3 \rightarrow 1$ and $3 \rightarrow 2$ transitions, respectively.

(v) H_{EP} describes the driving of the cavity pump mode by a classical field of amplitude $\overline{\varepsilon}$ and frequency ω_p.

(vi) H_{PD} and H_{RD} describe leakage of the pump and Raman fields from the cavity. The reservoir operators for energy dissipation are $\hat{\xi}_p$ and $\hat{\xi}_r$, respectively.

(vii) H_{A_1D} describes spontaneous emission on both the pump and Raman transitions, with reservoir operators $\hat{\Xi}_p$ and $\hat{\Xi}_r$.

(viii) H_{A_2D} describes dephasing of the atomic level populations due to elastic collisions. $\hat{\zeta}_1$, $\hat{\zeta}_2$, $\hat{\zeta}_3$, are the reservoir operators associated with this process.

(ix) H_{A_3D} describes population transfer between the two lower states due to inelastic collisions. Here $\hat{\eta}_1$ and $\hat{\eta}_2$ are the reservoir operators. The $1 \rightarrow 2$ transition is modeled by a negative temperature heat bath [23].

From this Hamiltonian a master equation for the atom-field system (where reservoir operators have been traced out) can easily be written down using standard techniques [23] and is given as follows:

$$\dot{\rho} = \frac{-i}{\hbar} [H_{PF} + H_{RF} + H_{AF} + H_{AP} + H_{AR} + H_{EP}, \rho] \tag{16}$$

$$+ \mathcal{L}_{PD}\rho + \mathcal{L}_{RD}\rho + \mathcal{L}_{A_1D}\rho + \mathcal{L}_{A_2D}\rho + \mathcal{L}_{A_3D}\rho, \tag{17}$$

where

$$\mathcal{L}_{PD}\rho=\frac{\bar{\kappa}}{2}(n_p^l+1)(2\hat{p}\rho\hat{p}^\dagger-\hat{p}^\dagger\hat{p}\rho-\rho\hat{p}^\dagger\hat{p})+\frac{\bar{\kappa}}{2}n_p^l(2\hat{p}^\dagger\rho\hat{p}-\hat{p}\hat{p}^\dagger\rho-\rho\hat{p}\hat{p}^\dagger), \tag{18}$$

$$\mathcal{L}_{RD}\rho=\frac{\bar{\kappa}}{2}(n_r^l+1)(2\hat{r}\rho\hat{r}^\dagger-\hat{r}^\dagger\hat{r}\rho-\rho\hat{r}^\dagger\hat{r})+\frac{\bar{\kappa}}{2}n_r^l(2\hat{r}^\dagger\rho\hat{r}-\hat{r}\hat{r}^\dagger\rho-\rho\hat{r}\hat{r}^\dagger), \tag{19}$$

$$\mathcal{L}_{A_1D}\rho=\sum_{\mu=1}^{N}\frac{\bar{\gamma}_p}{2}(1+n_p^{sp})(2\hat{\sigma}_{13}^{\mu}\rho\hat{\sigma}_{13}^{\mu\dagger}-\hat{\sigma}_{33}^{\mu}\rho-\rho\hat{\sigma}_{33}^{\mu})+\frac{\bar{\gamma}_p}{2}n_p^{sp}(2\hat{\sigma}_{13}^{\mu\dagger}\rho\hat{\sigma}_{13}^{\mu}-\hat{\sigma}_{11}^{\mu}\rho-\rho\hat{\sigma}_{11}^{\mu})+\frac{\bar{\gamma}_r}{2}(1+n_r^{sp})(2\hat{\sigma}_{23}^{\mu}\rho\hat{\sigma}_{23}^{\mu\dagger}-\hat{\sigma}_{33}^{\mu}\rho-\rho\hat{\sigma}_{33}^{\mu})+\frac{\bar{\gamma}_r}{2}n_r^{sp}(2\hat{\sigma}_{23}^{\mu\dagger}\rho\hat{\sigma}_{23}^{\mu}-\hat{\sigma}_{22}^{\mu}\rho-\rho\hat{\sigma}_{22}^{\mu}), \tag{20}$$

$$\mathcal{L}_{A_2D}\rho=\sum_{\mu=1}^{N}\frac{\bar{\kappa}_3}{2}(2\hat{\sigma}_{33}^{\mu}\rho\hat{\sigma}_{33}^{\mu}-\hat{\sigma}_{33}^{\mu}\rho-\rho\hat{\sigma}_{33}^{\mu})+\frac{\bar{\kappa}_2}{2}(2\hat{\sigma}_{22}^{\mu}\rho\hat{\sigma}_{22}^{\mu}-\hat{\sigma}_{22}^{\mu}\rho-\rho\hat{\sigma}_{22}^{\mu})+\frac{\bar{\kappa}_1}{2}(2\hat{\sigma}_{11}^{\mu}\rho\hat{\sigma}_{11}^{\mu}-\hat{\sigma}_{11}^{\mu}\rho-\rho\hat{\sigma}_{11}^{\mu}), \tag{21}$$

$$\mathcal{L}_{A_3D}\rho=\sum_{\mu=1}^{N}\frac{\bar{\Gamma}_2}{2}(2\hat{\sigma}_{12}^{\mu}\rho\hat{\sigma}_{12}^{\mu\dagger}-\hat{\sigma}_{22}^{\mu}\rho-\rho\hat{\sigma}_{22}^{\mu})+\frac{\bar{\Gamma}_1}{2}(2\hat{\sigma}_{12}^{\mu\dagger}\rho\hat{\sigma}_{12}^{\mu}-\hat{\sigma}_{11}^{\mu}\rho-\rho\hat{\sigma}_{11}^{\mu}). \tag{22}$$

The coefficients $\bar{\gamma}_p$ and $\bar{\gamma}_r$ are the Einstein A rates for the pump and Raman transitions, respectively, and the cavity decay rates for the pump and Raman fields have been assumed to be equal and are denoted by $\bar{\kappa}$. The atomic dephasing rates $\bar{\kappa}_1$, $\bar{\kappa}_2$, and $\bar{\kappa}_3$ (associated with states 1, 2, and 3, respectively), and the transfer rates $\bar{\Gamma}_1$ (from $1\rightarrow2$) and $\bar{\Gamma}_2$ (from $2\rightarrow1$) incorporate the thermal bath perturber number. The thermal photon numbers n_p^l and n_r^l (associated with leakage of pump and Raman photons from the cavity), and $n_p^{\rm sp}$ and $n_r^{\rm sp}$ (associated with spontaneous emission on the pump and Raman transitions) have been included for generality, but are small at optical frequencies and will henceforth be neglected.

III. THE FOKKER-PLANCK EQUATION

We now derive an equation of motion for the quasiprobability function, $P(\mathbf{Z})$, where $\mathbf{Z}=(\bar{\alpha},\bar{\alpha}^\dagger,\bar{\beta},\bar{\beta}^\dagger,\bar{J}_{13}^{+},\bar{J}_{13}^{-},\bar{J}_{23}^{+},\bar{J}_{23}^{-},\bar{J}_{12}^{+},\bar{J}_{12}^{-},\bar{D}_{31},\bar{D}_{32})$ are the c-number equivalents of the atomic and field operators. The resulting equation has the form of a Fokker-Planck equation (FPE), and is obtained via the equation of motion for the characteristic function $\chi(\boldsymbol{\lambda})$, which is defined in terms of the density matrix as

$$\chi(\boldsymbol{\lambda})=\mathrm{Tr}\{\rho O(\boldsymbol{\lambda})\}=\mathrm{Tr}\{\rho O^A(\boldsymbol{\lambda})O^F(\boldsymbol{\lambda})\}, \tag{23}$$

where $\boldsymbol{\lambda}=(\lambda_1,\lambda_2,\lambda_3,\lambda_4,\lambda_5,\lambda_6,\lambda_7,\lambda_8,\lambda_9,\lambda_{10},\lambda_{11},\lambda_{12})$ is the Fourier-space equivalent of the c numbers $\mathbf{Z}$, and $O(\boldsymbol{\lambda})$ is a product of exponential operators involving $\boldsymbol{\lambda}$ and the system operators.

A derivation of the FPE, using the approach due to Haken [20], has been commonly used with two-state atomic systems [21], but gives rise to ambiguities in the operator ordering when applied to three-level systems. We have therefore applied the phase-space methods of Smith and Gardiner [22], who have shown that the product of exponentials of operators, $O^A(\boldsymbol{\lambda})$, appearing in the definition of $\chi(\boldsymbol{\lambda})$ and used by Haken, can be written equivalently as a product of a linear combination of operators,

$$O^A(\boldsymbol{\lambda})=\prod_{\mu=1}^{N}(Q+q_1\hat{D}_{31}^{\mu}+q_2\hat{D}_{32}^{\mu}+c_{12}^{+}\hat{S}_{12}^{+\mu}+c_{13}^{+}\hat{S}_{13}^{+\mu}+c_{23}^{+}\hat{S}_{23}^{+\mu}+c_{12}^{-}\hat{S}_{12}^{-\mu}+c_{13}^{-}\hat{S}_{13}^{-\mu}+c_{23}^{-}\hat{S}_{23}^{-\mu}), \tag{24}$$

where

$$\hat{D}_{ij}^{\mu}\equiv\hat{\sigma}_{ii}^{\mu}-\hat{\sigma}_{jj}^{\mu}, \tag{25}$$

$$\hat{S}_{13}^{-\mu}\equiv\hat{\sigma}_{13}^{\mu}e^{-i\mathbf{k}_p\cdot\mathbf{r}_\mu}, \tag{26}$$

$$\hat{S}_{23}^{-\mu}\equiv\hat{\sigma}_{23}^{\mu}e^{-i\mathbf{k}_r\cdot\mathbf{r}_\mu}, \tag{27}$$

$$\hat{S}_{12}^{-\mu}\equiv\hat{\sigma}_{12}^{\mu}e^{-i(\mathbf{k}_p-\mathbf{k}_r)\cdot\mathbf{r}_\mu}, \tag{28}$$

and $\hat{S}_{ij}^{+\mu}=(\hat{S}_{ij}^{-\mu})^\dagger$. In the above definitions, individual atoms are labeled by the index μ, and their positions are $\mathbf{r}_\mu$. The variables Q, q_1, q_2, $\mathbf{c}^+$, and $\mathbf{c}^-$ are combinations of the λ_i's. Since the field operators do not have the ordering problems of the atomic operators, $O^F(\boldsymbol{\lambda})$ retains the original form

$$O^F(\boldsymbol{\lambda})=e^{i\lambda_4\hat{p}^\dagger}e^{i\lambda_3\hat{r}^\dagger}e^{i\lambda_2\hat{r}}e^{i\lambda_1\hat{p}}.$$

This description of the atomic part of the system contains nine variables, of which one is redundant and needs to be eliminated, since it gives rise to diffusion terms for which there are no corresponding drift terms. Smith and Gardiner provide a substitution which eliminates this redundant variable [22],

$$\chi=Q^N f(i\lambda_1,i\lambda_2,i\lambda_3,i\lambda_4,q_1/Q,q_2/Q,\mathbf{c}^+/Q,\mathbf{c}^-/Q)=Q^N f(i\lambda_1,i\lambda_2,i\lambda_3,i\lambda_4,y_1,y_2,\mathbf{x}^+,\mathbf{x}^-). \tag{29}$$

Upon replacing χ on both sides of the equation

$$\dot{\chi}(\boldsymbol{\lambda}) = \mathrm{Tr}\{\dot{\rho} O(\boldsymbol{\lambda})\}$$

with Eq. (29), the variable Q is eliminated, leaving an equation of motion for f, the reduced characteristic function. The 12-dimensional Fourier transform of the equation of motion for f will yield an equation of motion for $P(\mathbf{Z})$, and can be arrived at via the following correspondences:

$$i\lambda_1 \rightarrow -\frac{\partial}{\partial \bar{\alpha}}, \quad \frac{\partial}{\partial i\lambda_1} \rightarrow \bar{\alpha},$$

$$i\lambda_2 \rightarrow -\frac{\partial}{\partial \bar{\beta}}, \quad \frac{\partial}{\partial i\lambda_2} \rightarrow \bar{\beta},$$

$$i\lambda_3 \rightarrow -\frac{\partial}{\partial \bar{\beta}^\dagger}, \quad \frac{\partial}{\partial i\lambda_3} \rightarrow \bar{\beta}^\dagger,$$

$$i\lambda_4 \rightarrow -\frac{\partial}{\partial \bar{\alpha}^\dagger}, \quad \frac{\partial}{\partial i\lambda_4} \rightarrow \bar{\alpha}^\dagger,$$

$$x_{ij}^{\pm} \rightarrow -\frac{\partial}{\partial \bar{J}_{ij}^{\pm}}, \quad \frac{\partial}{\partial x_{ij}^{\pm}} \rightarrow \bar{J}_{ij}^{\pm},$$

$$y_1 \rightarrow -\frac{\partial}{\partial \bar{D}_{31}}, \quad \frac{\partial}{\partial y_1} \rightarrow \bar{D}_{31},$$

$$y_2 \rightarrow -\frac{\partial}{\partial \bar{D}_{32}}, \quad \frac{\partial}{\partial y_2} \rightarrow \bar{D}_{32},$$

where $\bar{\alpha}$, $\bar{\beta}$, $\bar{J}_{ij}^{\pm}$, and $\bar{D}_{ij}$ are c numbers corresponding to the operators $\hat{p}$, $\hat{r}$, $\hat{S}_{ij}^{\pm} = \Sigma_\mu \hat{S}_{ij}^{\pm\mu}$, and $\hat{D}_{ij} = \Sigma_\mu \hat{D}_{ij}^{\mu}$, respectively. Here the bars simply indicate that these c numbers are not in a rotated frame, and they will be dropped later when the system is transformed into one.

For the sake of completeness and correctness, we have used the positive-P representation [23] in writing down the above correspondences, so that we have 12 independent complex operators. In this representation, operators and their adjoints cannot be considered as necessarily being complex conjugate, however for simplicity we will later restrict our attention to such a classical subspace.

The resulting equation of motion for the distribution function $P(\mathbf{Z})$ is rather lengthy, and is thus given in Appendix A. It contains terms up to third order in the derivatives, however we can show that these third-order terms are small by introducing the scaling [23]

$$\tilde{\alpha} = \frac{\bar{\alpha}}{\sqrt{N}}, \quad \tilde{\beta} = \frac{\bar{\beta}}{\sqrt{N}}, \quad \tilde{\varepsilon} = \frac{\bar{\varepsilon}}{\sqrt{N}}, \quad \tilde{J}_{ij}^{+} = \frac{\bar{J}_{ij}^{+}}{N},$$

$$\tilde{J}_{ij}^{-} = \frac{\bar{J}_{ij}^{-}}{N}, \quad \tilde{D}_{ij} = \frac{\bar{D}_{ij}}{N}, \quad \tilde{g}_p = \bar{g}_p \sqrt{N}. \tag{30}$$

With this substitution, drift terms are independent of N, second derivative terms are proportional to $1/N$, and third-order terms are proportional to $1/N^2$. In the atomic system we consider here, N is large enough that the third-order terms can be neglected. Dropping these terms gives us the FPE which can be made dimensionless by rescaling the time to $\tau = t\bar{\gamma}_\perp^{12}$, where $\bar{\gamma}_\perp^{12}$ is an overall decay rate for the dipole between states 1 and 2, and its definition in terms of previously introduced quantities is given in Appendix A. All rates and frequencies (including $\tilde{\varepsilon}$ and $\tilde{g}_i$) are then rescaled in terms of $\bar{\gamma}_\perp^{12}$, and this scaling is indicated by removing the bar (or tilde) from each quantity. From this FPE, quantum stochastic differential equations (QSDEs) can be written down, and then transforming to a rotating frame, for which

$$\tilde{\alpha}^\dagger e^{-i\omega_p t} \rightarrow \alpha^\dagger, \quad \tilde{\alpha} e^{i\omega_p t} \rightarrow \alpha,$$

$$\tilde{\beta}^\dagger e^{-i\omega_r t} \rightarrow \beta^\dagger, \quad \tilde{\beta} e^{i\omega_r t} \rightarrow \beta,$$

$$\tilde{J}_{13}^{+} e^{-i\omega_p t} \rightarrow J_{13}^{+}, \quad \tilde{J}_{13}^{-} e^{i\omega_p t} \rightarrow J_{13}^{-},$$

$$\tilde{J}_{23}^{+} e^{-i\omega_r t} \rightarrow J_{23}^{+}, \quad \tilde{J}_{23}^{-} e^{i\omega_r t} \rightarrow J_{23}^{-},$$

$$\tilde{J}_{12}^{+} e^{-i(\omega_p - \omega_r)t} \rightarrow J_{12}^{+}, \quad \tilde{J}_{12}^{-} e^{i(\omega_p - \omega_r)t} \rightarrow J_{12}^{-},$$

$$\tilde{D}_{31} \rightarrow D_{31}, \quad \tilde{D}_{32} \rightarrow D_{32},$$

we finally obtain the stochastic equations,

$$\dot{\alpha} = g_p J_{13}^{-} - \frac{\kappa}{2}\alpha + i\phi_1 \alpha + \varepsilon + \frac{\Gamma_\alpha}{\sqrt{N}}, \tag{31}$$

$$\dot{\alpha}^\dagger = g_p^* J_{13}^{+} - \frac{\kappa}{2}\alpha^\dagger - i\phi_1 \alpha^\dagger + \varepsilon^* + \frac{\Gamma_{\alpha^\dagger}}{\sqrt{N}}, \tag{32}$$

$$\dot{\beta} = g_r J_{23}^{-} - \frac{\kappa}{2}\beta + i(\phi_2 + \Delta')\beta + \frac{\Gamma_\beta}{\sqrt{N}}, \tag{33}$$

$$\dot{\beta}^\dagger = g_r^* J_{23}^{+} - \frac{\kappa}{2}\beta^\dagger - i(\phi_2 + \Delta')\beta^\dagger + \frac{\Gamma_{\beta^\dagger}}{\sqrt{N}}, \tag{34}$$

$$\dot{J}_{12}^{+} = i\Delta' J_{12}^{+} + g_p J_{23}^{-}\alpha^\dagger + g_r^* J_{13}^{+}\beta - J_{12}^{+} + \frac{\Gamma_{J_{12}^{+}}}{\sqrt{N}}, \tag{35}$$

$$\dot{J}_{12}^{-} = -i\Delta' J_{12}^{-} + g_p^* J_{23}^{+}\alpha + g_r J_{13}^{-}\beta^\dagger - J_{12}^{-} + \frac{\Gamma_{J_{12}^{-}}}{\sqrt{N}}, \tag{36}$$

$$\dot{J}_{13}^{+} = -i\Delta J_{13}^{+} + g_p D_{31}\alpha^\dagger - g_r J_{12}^{+}\beta^\dagger - \gamma_\perp^{13} J_{13}^{+} + \frac{\Gamma_{J_{13}^{+}}}{\sqrt{N}}, \tag{37}$$

$$\dot{J}_{13}^{-} = i\Delta J_{13}^{-} + g_p^* D_{31}\alpha - g_r^* J_{12}^{-}\beta - \gamma_\perp^{13} J_{13}^{-} + \frac{\Gamma_{J_{13}^{-}}}{\sqrt{N}}, \tag{38}$$

$$\dot{J}_{23}^{+}=-i\Delta_r J_{23}^{+}-g_p J_{12}^{-}\alpha^{\dagger}+g_r D_{32}\beta^{\dagger}-\gamma_{\perp}^{23}J_{23}^{+}+\frac{\Gamma_{J_{23}^{+}}}{\sqrt{N}}, \tag{39}$$

$$\dot{J}_{23}^{-}=i\Delta_r J_{23}^{-}-g_p^{*}J_{12}^{+}\alpha+g_r^{*}D_{32}\beta-\gamma_{\perp}^{23}J_{23}^{-}+\frac{\Gamma_{J_{23}^{-}}}{\sqrt{N}}, \tag{40}$$

$$\dot{D}_{31}=-2g_p J_{13}^{-}\alpha^{\dagger}-2g_p^{*}J_{13}^{+}\alpha-g_r J_{23}^{-}\beta^{\dagger}-g_r^{*}J_{23}^{+}\beta+r_0+r_1 D_{31}+r_2 D_{32}+\frac{\Gamma_{D_{31}}}{\sqrt{N}}, \tag{41}$$

$$\dot{D}_{32}=-g_p J_{13}^{-}\alpha^{\dagger}-g_p^{*}J_{13}^{+}\alpha-2g_r J_{23}^{-}\beta^{\dagger}-2g_r^{*}J_{23}^{+}\beta+s_0+s_1 D_{31}+s_2 D_{32}+\frac{\Gamma_{D_{32}}}{\sqrt{N}}, \tag{42}$$

where $\phi_1=(\omega_p-\omega_p^c)/\overline{\gamma_{\perp}^{12}}$ and $\phi_2=(\omega_r-\omega_r^c)/\overline{\gamma_{\perp}^{12}}$ and all other definitions of symbols (in their unscaled form) have been given in Appendix A or Sec. II. The Γ_i represent the noise terms, whose correlations are given in Appendix B.

The deterministic parts of these equations can be shown to reduce, in the classical subspace [24] (where $\alpha^{\dagger}=\alpha^{*}$), to those given by Xia *et al.* [19] as expected.

IV. STEADY-STATE SOLUTIONS

In the positive-*P* representation, there are 24 variables in our system, for which we need to find steady-state solutions. However, because of the detunings in the problem, it is very difficult to find steady-state solutions outside the classical subspace, and so we restrict our attention to the 12 variable regime in which $\alpha^{\dagger}=\alpha^{*}$, $\beta^{\dagger}=\beta^{*}$, $(J_{ij}^{+})^{*}=J_{ij}^{-}$, and $(D_{ij})^{*}=D_{ij}$. Making this assumption gives QSDEs, which are the same as those that would be obtained if the Glauber-Sudarshan *P* representation were used. Within a linearized analysis our results should not be affected by limiting our attention to the classical subspace, since departure from these solutions is expected only when the quantum noise becomes large. Thus the diffusion matrix remains positive semidefinite and the eigenvalues non-negative, provided we restrict ourselves to the regime in which the linearization is valid. Even with this simplification, a numerical approach is required to solve for the system in steady state.

The first step in solving the equations is to eliminate the unknown Raman frequency ω_r from the problem, since it is determined by the system itself and will change as the lasing conditions change. The elimination can be accomplished by transforming the QSDEs into a new set of fifteen equations in the following variables [25]:

$$\begin{aligned}
U_1&=|\beta|^2,\\
U_3+iU_2&=2\alpha,\\
U_7+iU_4&=2J_{13}^{-},\\
U_8+iU_5&=2\beta J_{23}^{+},\\
U_9+iU_6&=2\beta J_{12}^{-},\\
U_{10}&=D_{31},\\
U_{11}&=D_{32},\\
U_{12}&=J_{23}^{+}J_{23}^{-},\\
U_{14}+iU_{13}&=2J_{12}^{-}J_{23}^{-},\\
U_{15}&=J_{12}^{+}J_{12}^{-}.
\end{aligned} \tag{43}$$

The Raman frequency ω_r is not present in these variables and we now have 15 equations and 15 unknowns. These are given in Appendix C. In converting the scaled QSDEs to U_i variables, we have ignored the Ito contributions [26] which arise. This is a valid approximation, since the Ito contributions are of order N^{-1} smaller than the dominant QSDE contributions. We have used the package AUTO [27] in order to solve the deterministic parts of these equations in the steady state, and to perform a stability analysis on the solutions.

V. LINEARIZATION OF STOCHASTIC EQUATIONS

We will be interested in calculating the intensity noise spectrum of both the pump and the Raman fields, thus we eliminate the pump field variables U_2 and U_3 in favor of intensity and phase variables, using

$$I_{\alpha}=\frac{U_3^2+U_2^2}{4},$$

$$\phi_{\alpha}=\frac{1}{2i}\ln\left[\frac{U_3+iU_2}{2}\right].$$

We emphasize that the Raman phase does not appear in the resulting system of equations, since it has been explicitly eliminated.

The QSDEs are linearized about the steady-state U_i, I_{α}, and ϕ_{α} values to first order in $1/\sqrt{N}$, according to

$$\mathbf{U}=\mathbf{U}^0+\frac{\delta\mathbf{U}}{\sqrt{N}},$$

$$I_{\alpha}=I_{\alpha}^0+\frac{\delta I_{\alpha}}{\sqrt{N}},$$

$$\phi_{\alpha}=\phi_{\alpha}^0+\frac{\delta\phi_{\alpha}}{\sqrt{N}},$$

and the resulting equations have the form

$$\begin{pmatrix} d\,\delta\mathbf{U}(t)\\ d\,\delta I_{\alpha}(t)\\ d\,\delta\phi_{\alpha}(t)\end{pmatrix}=-A\begin{pmatrix}\delta\mathbf{U}(t)\\ \delta I_{\alpha}(t)\\ \delta\phi_{\alpha}(t)\end{pmatrix}dt+B\,d\mathbf{W}(t), \tag{44}$$

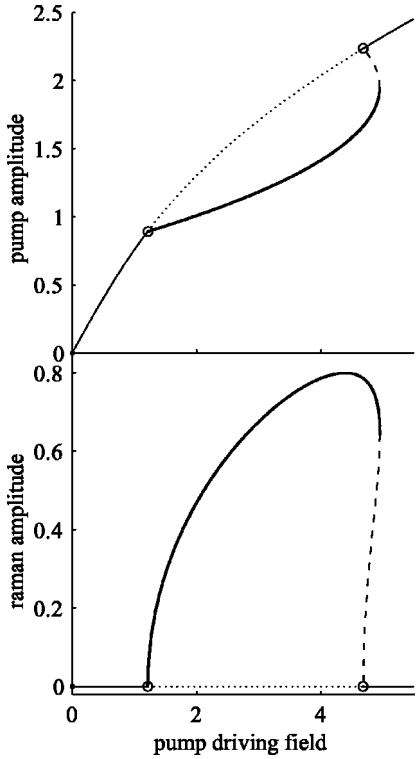

FIG. 2. Pump and Raman input-output curves. The intracavity pump and Raman output amplitudes, $|\alpha|$ and $|\beta|$ respectively, are plotted on the vertical axes, and the pump input field $2\varepsilon/\kappa$ is plotted horizontally. The branches corresponding to the nonzero Raman field are indicated by heavy solid lines (stable region) and dashed lines (unstable region). The branches corresponding to the zero Raman field are indicated by lighter solid lines (stable) and dotted lines (unstable). The threshold points for Raman lasing are indicated by the open circles. Parameters are $\gamma_{\perp}^{13}=1$, $\gamma_{\perp}^{23}=1$, $\Gamma_1=0.065$, $\Gamma_2=0.8$, $\gamma_p=0.058$, $\gamma_r=0.025$, $g_p=23.66$, $g_r=16.73$, $\kappa=0.4$, $\phi_1=-1$, $\phi_2=1.5$, $\Delta=-600$.

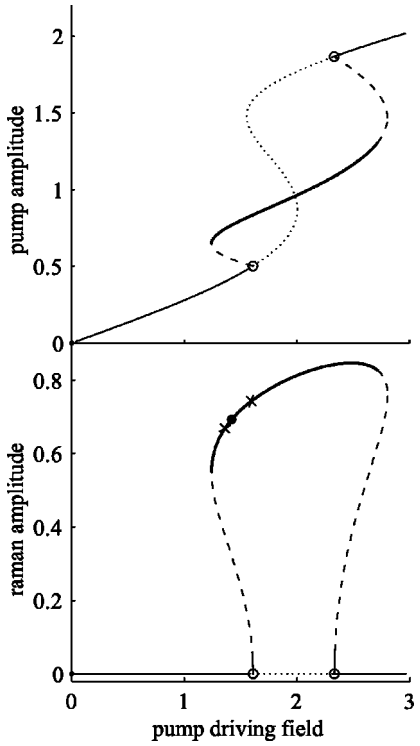

FIG. 3. Pump and Raman input-output curves. Parameters are the same as for Fig. 2 except that $\Delta=-300$. The range of squeezing is indicated by crosses, and the point of best squeezing by a closed circle.

where A is the drift matrix and BB^T the diffusion matrix of the system, both easily obtained from the FPE.

VI. DETERMINISTIC SYSTEM BEHAVIOR

A detailed analysis of the deterministic behavior of this Raman system as a function of input driving field has previously been carried out by Xia [25]. For the convenience of the reader we briefly review the main features of interest. A rich variety of behavior is found, and examples which represent typical behavior are shown in Figs. 2 and 3, where the output pump and Raman amplitudes are plotted against the input pump amplitude $2\varepsilon/\kappa$. (We note that all field amplitudes plotted are intracavity values.) In these figures, stable solutions are displayed as a solid line, and unstable solutions as dashed or dotted lines. It is easy to show [e.g, see Ref. [19], Eq. (17)] that the system always has a solution in which the Raman field is zero and the pump output obeys the equation of two-state optical bistability [19]. This ''two-state'' OB solution (which we call the 2OB branch) is shown by the curve made up of a thin solid line and a dotted line. However, in the region between the open circles, the 2OB branch is unstable and an additional, nonzero, Raman solution and the corresponding pump solution [shown as thick solid lines (where stable) and dashed lines (where unstable)] appear. In Fig. 3, where the 2OB branch has an S shape, the nonzero Raman solution and its associated pump solution show switching behavior at both the lower and upper threshold points.

The physics underlying the Raman switching behavior seen in Figs. 2 and 3 has been discussed by Xia [25] in terms of nonlinear coupling terms η and η_r, which are defined for the pump and Raman fields, respectively, as

$$\eta=-g_pJ_{13}^{-}/\alpha$$

and

$$\eta_r=-g_rJ_{23}^{-}/\beta.$$

$\mathrm{Re}(\eta)$ represents the (amplitude) loss coefficient and $\mathrm{Im}(\eta)$ the dispersive phase shift (or frequency pulling) for the pump field, while $-\mathrm{Re}(\eta_r)$ is the Raman (amplitude) gain coefficient and $\mathrm{Im}(\eta_r)$ the Raman frequency pulling. Xia *et al.* [19] have also shown that Raman switching in the context of frequency scanning can be understood in terms of the behavior of η and η_r. For the reader's convenience, we briefly outline the argument here as related to the intensity scans, using Fig. 3 as an example. We begin by describing the pump behavior. The solution branch for the pump is dominated by the behavior of the pump dispersion $\mathrm{Im}(\eta)$, since the pump detuning Δ is very large. The resonant cavity frequency ω_p^o for the pump is given by $\omega_p^o=\omega_p^c+\mathrm{Im}(\eta)$, but the pump frequency (which is externally determined) is set between ω_p^c and the unsaturated value of ω_p^o. In the absence of Raman lasing, $\mathrm{Im}(\eta)$ bleaches as the pump field intensity

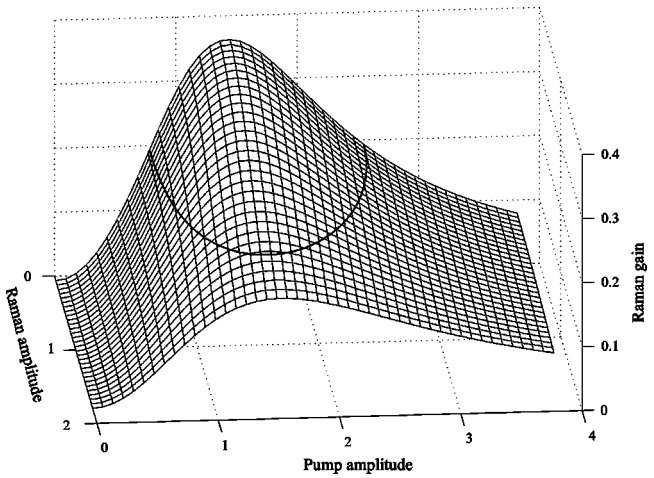

FIG. 4. Raman gain, $-\mathrm{Re}(\eta_r)$, as a function of pump and Raman field amplitudes for the parameters of Fig. 3.

increases, causing the cavity to become more resonant and the pump cavity field to grow. This positive feedback situation leads (under appropriate conditions) to an upward switch of the pump intensity. The steady-state behavior has a simple analytic description on the 2OB branch [19],

$$|\alpha|^2=\frac{|\varepsilon|^2}{[\kappa/2+\mathrm{Re}(\eta)]^2+[\phi_1-\mathrm{Im}(\eta)]^2}, \tag{45}$$

where η is given by Eq. (17) of [19], and ϕ_1 is the vacuum cavity detuning of the pump field. In the dispersive regime we are considering, the switching (i.e., the bend in the 2OB curve) occurs where the effective cavity intensity becomes sufficiently large to bleach the phase shift $\mathrm{Im}(\eta)$ to a value close to ϕ_1, thus allowing the cavity to become near resonant.

The Raman solution is driven by a different mechanism. Raman lasing occurs when there is sufficient Raman gain (for given pump intensity) to match the cavity loss, i.e.

$$-2\mathrm{Re}(\eta_r)=\kappa. \tag{46}$$

Raman frequency pulling is small in the regime of Fig. 3, and plays no significant role in the deterministic Raman output amplitude behavior. The Raman gain is therefore the key mechanism, and its behavior in the relevant regime is shown in Fig. 4, where it is plotted as a function of $|\alpha|$ and $|\beta|$, with all other parameters fixed at values corresponding to Fig. 3. The contour shows the trajectory that $|\alpha|$ and $|\beta|$ must follow to satisfy Eq. (46), and has endpoints at the lower and upper thresholds for Raman lasing. When the Raman field first turns on at the lower threshold, it contributes additional bleaching to the pump phase shift, causing an abrupt increase in pump amplitude (by the dispersive mechanism and feedback described above) and a corresponding jump (i.e., switch) occurs in the Raman field in order to remain on the contour of Fig. 3. As the pump input is further increased, the pump cavity field continues to increase, and the Raman field adjusts to an appropriate value, following the contour in Fig. 4. Eventually at high enough pump field, Raman lasing ceases.

VII. CALCULATION OF SQUEEZING SPECTRA

The majority of squeezing calculations in the optical bistability context have concentrated on quadrature phase fluctuations. In the case of a Raman laser, however, where the frequency of the output field is dependent on operating conditions, the local oscillator phase cannot be controlled, and so it is more appropriate to study the intensity fluctuations in the pump and Raman fields. Previous Raman squeezing papers have calculated the Mandel Q parameter, and inferred a Lorentzian squeezing spectrum. Here we calculate directly the intensity fluctuation spectrum internal to the cavity according to

$$S(\omega)=\frac{1}{2\pi}(A+i\omega)^{-1}BB^T(A^T-i\omega)^{-1},$$

in which A is the drift matrix and BB^T is the diffusion matrix, given by Eq. (44). We shall find that the spectrum is often not at all Lorentzian. The normalized variance of intensity fluctuations in mode j external to the cavity is obtained from the (j,j) element of the spectral matrix $S(\omega)$, as

$$V_{jj}(\omega)=1+2\pi\frac{\kappa S_{jj}(\omega)}{I_j^0}.$$

A value of $V_{jj}(\omega)$ of 1 corresponds to the shot-noise limit. For squeezed light $V_{jj}(\omega)$ is between 0 (perfectly squeezed light) and 1. In this paper we are only interested in the two components of $V_{jj}(\omega)$ corresponding to the pump field and the Raman field, which we will denote $V_\alpha(\omega)$ and $V_\beta(\omega)$, respectively.

VIII. SQUEEZING BEHAVIOR

We have numerically investigated the squeezing of the Raman and pump fields for a broad range of parameters, and in this section we survey the main behavior trends. This survey is intended to provide a good representation of broad classes of behavior: an exhaustive listing of all possible types of behavior is not practicable. We begin with the case shown in Fig. 3, which represents the most typical system behavior. Other types of behavior can be obtained by the systematic variation of parameters presented below. In Fig. 3, squeezing in the Raman field occurs in the range between the crosses. The smallest value of the spectral variance for these parameters was found at the point marked by the filled circle in Fig. 3 ($2\varepsilon/\kappa=1.42$), and the squeezing spectrum at this point is shown in Fig. 5 and is clearly not Lorentzian. The smallest value of $V_\beta(\omega)$ (which corresponds to the maximum squeezing) is 0.937 at frequencies $\omega=\pm 0.19$. The pump intensity fluctuations are also presented and show that no squeezing in the pump field occurs for this choice of system operating point.

A. Dependence on κ

As the cavity decay rate κ is reduced, Raman squeezing increases, an effect related to the increased Raman lasing that will then occur. The Raman output occurs over a wider range [since less gain is now required, see Eq. (46)], while the region of bistable behavior on the 2OB curve moves to

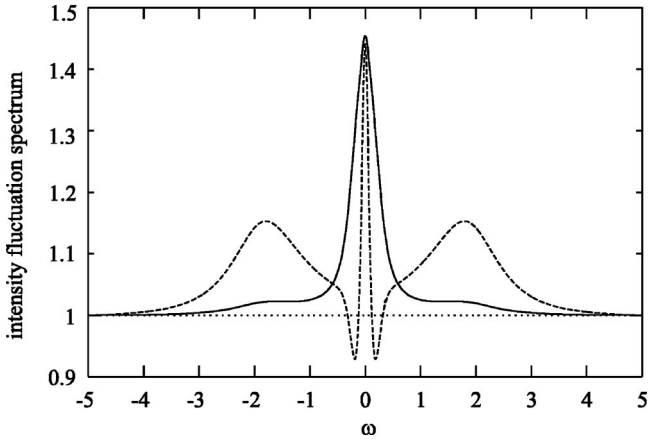

FIG. 5. Intensity fluctuation spectrum for pump, $V_\alpha(\omega)$ (solid line), and Raman, $V_\beta(\omega)$ (dashed line), output fields at the system operating point corresponding to the closed circle in Fig. 3. The dotted line indicates the shot-noise level.

higher intensities (because the unsaturated cavity pulling has increased). This is illustrated in Fig. 6, where κ has been set to 0.04, causing the Raman output curve to become a wider and taller loop than in Fig. 3. The increased stable range of the Raman output as κ is decreased leads to a larger range of pump driving field amplitudes over which Raman squeezing is found to occur.

The best squeezing is found for the lower driving field amplitudes on the stable part of the Raman branch, and as κ decreases from the value of 0.4 used in Fig. 3, the dips in the Raman squeezing spectra become deeper and narrower and move in towards $\omega=0$, as expected as the adiabatic limit is approached. At $\kappa=0.12$, the two dips coalesce into a single

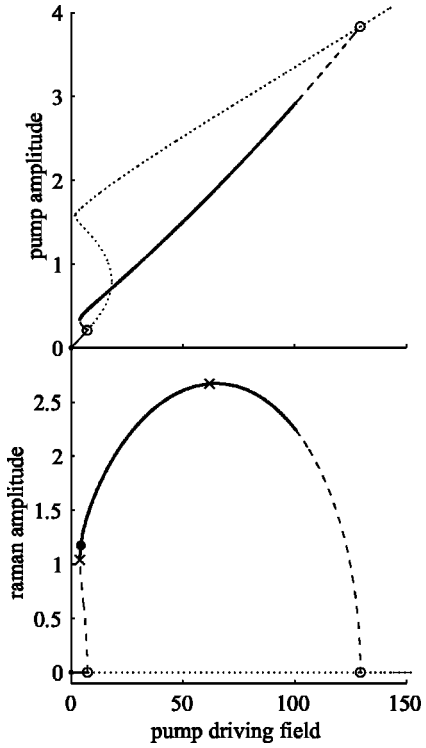

FIG. 6. Pump and Raman input-output curve with indicated squeezing range for $\kappa=0.04$. All other parameters are as in Fig. 3.

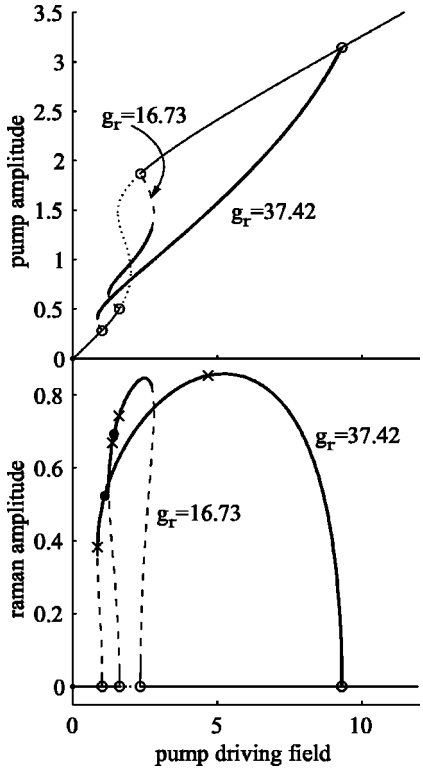

FIG. 7. Pump and Raman input-output curves with indicated squeezing ranges for $g_r=16.73$ and 37.42. All other parameters are as in Fig. 3.

one centered on $\omega=0$, where $V_\beta(0)=0.74$. No pump squeezing occurs with the choice of parameters in Fig. 3, for any value of κ. These results indicate that although squeezing is improved by operating in the good cavity limit, squeezing outside of this limit is also possible.

B. Dependence on g_r and g_p

As the Raman gain g_r increases, Raman squeezing improves. The 2OB curve is not altered by the changes in g_r, but the positions of the Raman threshold points are affected, moving further apart as g_r increases (as shown in Fig. 7), and moving closer together as g_r decreases, until Raman lasing ceases at $g_r=6.93$. No pump squeezing occurs for any change of g_r alone, but Raman squeezing increases in depth and occurs for a larger range of driving field as g_r increases to the value 118.32 [where $V_\beta(0)=0.694$ at pump field $2\varepsilon/\kappa=0.552$]. The best squeezing is found for the lower values of the stable part of the pump driving field range. Beyond $g_r=118.32$, $V_\beta(\omega)$ appears to saturate. Schernthanner and Ritsch [18] observed similar behavior using a simplified model of the Raman process.

As g_p is increased from the value used in Fig. 3, the Raman squeezing first improves, reaching a minimum variance of 0.75 for $g_p=28$, and then degrades rapidly as the length of the stable part of the Raman branch diminishes, and eventually disappears (at approximately $g_p=28.54$). Correspondingly, the 2OB input-output curve develops increasing nonlinearity as g_p increases, which is a well-known result [28]. When g_p is decreased from the value used in Fig. 3, Raman squeezing decreases, and then disappears at a value of g_p of about 23. A little below this value (at $g_p=22.94$),

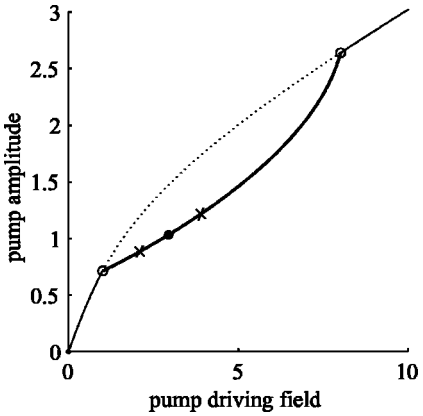

FIG. 8. Pump input-output curve with indicated squeezing range for $g_p = 16.73$. All other parameters are as in Fig. 3.

pump squeezing begins to appear, and occurs only on the pump branch corresponding to the nonzero Raman field. Pump squeezing is maximum (variance of 0.933) at $g_p = 21.27$, but persists to lower g_p values, even when the 2OB curve is no longer bistable, as illustrated in Fig. 8 where $g_p = 16.73$.

C. Variation of atomic decay rates

The main sensitivity of the system to the atomic rates is that positive Raman gain requires $\Gamma_2 > \Gamma_1$, and this gain increases as the difference between these two rates increases. Changing Γ_2 and Γ_1 through the values that allow Raman gain causes only minor changes to the curves in Fig. 3, with Raman output increasing as either Γ_2 increases or Γ_1 decreases. Raman squeezing occurs for almost all values of Γ_1 and Γ_2 that allow Raman gain, provided Γ_1 does not become larger than approximately 0.1 [we note that with the chosen scaling (in terms of $\gamma_\perp^{12}$), Γ_1, Γ_2 are limited to values between 0 and 2]. Optimal Raman squeezing occurs for $\Gamma_2 = 1$ and $\Gamma_1 = 0$, where for a pump amplitude of $2\varepsilon/\kappa = 1.66$, $V_\beta(\pm 0.24) = 0.8123$. Pump squeezing has an optimal value of $V_\alpha(\omega) = 0.892$ at $2\varepsilon/\kappa = 1.57$, when $\Gamma_1 = 0$ and $\Gamma_2 = 1$, and may coexist with Raman squeezing (provided $\Gamma_1 \lesssim 0.05$ and Γ_2 is in the range 0.7–1).

Changing one of γ_p or γ_r over a large range has only a minor effect on the deterministic input-output curves. Under change of γ_p, Raman squeezing exists for $0.03 \leqslant \gamma_p \leqslant 0.975$ and its optimum value of $V_\beta(0) = 0.674$ occurs at the upper end of this range, $\gamma_p = 0.975$, and $2\varepsilon/\kappa = 1.88$. Pump squeezing, on the other hand, occurs only if $\gamma_p \leqslant 0.02$, and achieves a best value of 0.9428 for $\gamma_p \to 0$. Under change of γ_r, Raman squeezing exists for $0 < \gamma_r \leqslant 0.942$ and its optimum value of $V_\beta(\omega) = 0.697$ occurs for $\gamma_r = 0.942$, $2\varepsilon/\kappa = 1.806$, $\omega = 0$. We note that pump squeezing does not occur while γ_p retains the value it has in Fig. 3 ($\gamma_p = 0.058$).

Given the choice of population decay rates in Fig. 3, $\gamma_\perp^{13}$ may be reduced to of order 0.1 but $\gamma_\perp^{23}$ cannot be decreased below about 0.5. When increasing these rates, it is realistic that both should be increased together, and this causes the switching region of the 2OB curve to move to smaller values of input field. The Raman branch tends to move to lower regions on the 2OB curve as $\gamma_\perp^{ij}$ decreases, and to higher regions as $\gamma_\perp^{ij}$ increases. For example, at small $\gamma_\perp^{13}$, the Raman threshold points are both on the lower branch of the 2OB curve, while for $\gamma_\perp^{13} = \gamma_\perp^{23} = 5$ the lower Raman threshold is in the negative slope region of the 2OB curve, and the upper threshold is on the upper 2OB branch. At small values of $\gamma_\perp^{13}$, both pump and Raman squeezing may coexist. For values of $\gamma_\perp^{13}$ and $\gamma_\perp^{23}$ above those in Fig. 3, no pump squeezing occurs, and Raman squeezing gradually disappears.

D. Variation of Δ, ϕ_1, and ϕ_2

Raman gain is favored at large pump detuning, and we have concentrated on this regime in this paper. For large Δ, pump switching is dominated by the dispersive mechanism, and is characterized chiefly by the unsaturated frequency pulling which in this regime behaves as Δ^{-1}, as does the Raman gain. The form of the system behavior can thus be preserved under large changes in Δ, provided corresponding modifications are made to the cavity detunings and the pump and Raman gain coefficients. For example, increasing $|\Delta|$ decreases the unsaturated frequency pulling, which must be compensated by increasing the pump gain g_p. Since the effective pump intensity decreases as Δ^{-2}, the required increase in g_p is more than linear, which in turn requires that pump frequency be moved further away from the empty cavity resonance. For the Raman field, gain is reduced due to the increase in $|\Delta|$ and must be compensated by increasing g_r. The Raman switching behavior is preserved by adjusting ϕ_2 in the same direction as ϕ_1. For example, the input-output system behavior shown in Fig. 3 can be essentially repro-

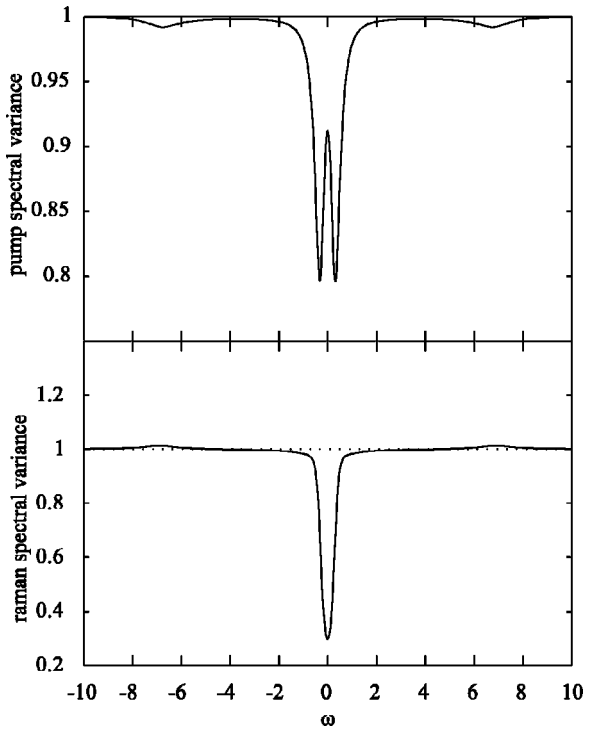

FIG. 9. Intensity fluctuation spectra $V_\alpha(\omega)$ and $V_\beta(\omega)$ for the case in which we found the greatest Raman squeezing of 0.2982. Parameters are $\gamma_\perp^{13} = 1.111$, $\gamma_\perp^{23} = 1.907$, $\Gamma_1 = 0$, $\Gamma_2 = 1.751$, $\gamma_p = 1.270$, $\gamma_r = 0.547$, $g_p = 51.810$, $g_r = 36.635$, $\kappa = 0.219$, $\phi_1 = -2.19$, $\phi_2 = 3.28$, $\Delta = -656.814$.

duced for a choice of parameters $\Delta=-600$, $g_p=47.75$, $\phi_1=-2.95$, $g_r=18.97$, $\phi_2=0.2$.

E. General observations

Some simple overall characteristics of the pump and Raman squeezing behavior have been observed in all parameter regimes examined. First, Raman squeezing is only seen when switching behavior is present, whereas pump squeezing may be found even when no bistability or switching behavior is present, (e.g., Fig. 8). Both Raman and pump squeezing are found only on parts of the input-output curve with positive slope, and the regions may overlap, but pump squeezing generally occurs at lower pump driving fields than Raman squeezing. The lowest value of Raman intensity spectral variance that we have found in our extensive parameter search is the value $V_\beta(0)=0.2982$ (see Fig. 9), which is greater Raman squeezing than has been previously reported.

IX. CONCLUSION

Previous treatments of squeezing in Raman lasers [13–18] employed simplified models which only cover a limited regime of the atomic or field dynamics. We have presented a more complex model which includes a quantum description of the pump field and treats the effects of the atom and field dynamics on the quantum noise. The equations which arise are correspondingly more complex than they were previously, and require numerical solution. From the results of an extensive investigation of the system behavior, in which the squeezing spectrum is directly calculated, we have found that the model gives enhanced regimes and quality of squeezing compared to earlier models. Squeezing occurs predominantly in the switching regime, and may also occur outside the good cavity limit. Neither of these regimes have been previously considered. Both the transmitted pump field and the Raman field may exhibit squeezing behavior, sometimes in coexistence.

We have explored in some detail the dependence of pump and Raman squeezing on the various system parameters and we have shown that squeezing improves as (i) the cavity decay rate decreases, (ii) pump gain increases, and (iii) Raman spontaneous decay rate γ_r increases. Our results also confirm the earlier observation [18] that Raman squeezing increases as the Raman gain increases. By calculating the squeezing spectrum directly, we have found it need not be Lorentzian. Finally, although perfect squeezing has not been found, we have shown that very low values of the spectral variance are possible.

ACKNOWLEDGMENTS

We thank Crispin Gardiner and Craig Savage for valuable discussions. This work was supported under FRST Contract No. UOO613.

APPENDIX A

We present the complete equation of motion for $P(\mathbf{Z})$ in the positive-P representation obtained using the method of Smith and Gardiner [22]. The first-order terms begin on line (A1a), the second-order terms on line (A1b), and the third-order terms on line (A1c):

$$\frac{\partial P(\mathbf{Z})}{\partial t}=\left\{ -\frac{\partial}{\partial\alpha}\left(-i\omega_p\alpha-\frac{\kappa}{2}\alpha+g_pJ_{13}^-+\varepsilon\right)-\frac{\partial}{\partial\alpha^\dagger}\left(i\omega_p\alpha^\dagger-\frac{\kappa}{2}\alpha^\dagger+g_p^*J_{13}^++\varepsilon^*\right)\right. \tag{A1a}$$

$$-\frac{\partial}{\partial\beta}\left(-i\omega_r\beta-\frac{\kappa}{2}\beta+g_rJ_{23}^-\right)-\frac{\partial}{\partial\beta^\dagger}\left(i\omega_r\beta^\dagger-\frac{\kappa}{2}\beta^\dagger+g_r^*J_{23}^+\right)$$

$$-\frac{\partial}{\partial J_{13}^-}(-i\omega_{31}J_{13}^--\gamma_\perp^{13}J_{13}^-+g_p^*\alpha D_{31}-g_r^*\beta J_{12}^-)-\frac{\partial}{\partial J_{13}^+}(i\omega_{31}J_{13}^+-\gamma_\perp^{13}J_{13}^++g_p\alpha^\dagger D_{31}-g_r\beta^\dagger J_{12}^+)$$

$$-\frac{\partial}{\partial J_{23}^-}(-i\omega_{32}J_{23}^--\gamma_\perp^{23}J_{23}^--g_p^*\alpha J_{12}^++g_r^*\beta D_{32})-\frac{\partial}{\partial J_{23}^+}(i\omega_{32}J_{23}^+-\gamma_\perp^{23}J_{23}^+-g_p\alpha^\dagger J_{12}^-+g_r\beta^\dagger D_{32})$$

$$-\frac{\partial}{\partial J_{12}^-}(-i\omega_{21}J_{12}^--\gamma_\perp^{12}J_{12}^-+g_p^*\alpha J_{23}^++g_r\beta^\dagger J_{13}^-)-\frac{\partial}{\partial J_{12}^+}(i\omega_{21}J_{12}^+-\gamma_\perp^{12}J_{12}^++g_p\alpha^\dagger J_{23}^-+g_r^*\beta J_{13}^+)$$

$$-\frac{\partial}{\partial D_{31}}(r_0N+r_1D_{31}+r_2D_{32}-2g_p\alpha^\dagger J_{13}^--2g_p^*\alpha J_{13}^+-g_r\beta^\dagger J_{23}^--g_r^*\beta J_{23}^+)$$

$$-\frac{\partial}{\partial D_{32}}(s_0N+s_1D_{31}+s_2D_{32}-g_p\alpha^\dagger J_{13}^--g_p^*\alpha J_{13}^+-2g_r\beta^\dagger J_{23}^--2g_r^*\beta J_{23}^+)$$

$$-\frac{\partial^2}{\partial D_{31}\partial J_{13}^-}r_0J_{13}^--\frac{\partial^2}{\partial D_{31}\partial J_{13}^+}r_0J_{13}^+-\frac{\partial^2}{\partial D_{31}\partial J_{23}^-}r_0J_{23}^--\frac{\partial^2}{\partial D_{31}\partial J_{23}^+}r_0J_{23}^+ \tag{A1b}$$

$$
\begin{aligned}
&-\frac{\partial^2}{\partial\bar{D}_{31}\partial\bar{J}_{12}^-}\bar{r}_0\bar{J}_{12}^- - \frac{\partial^2}{\partial\bar{D}_{31}\partial\bar{J}_{12}^+}\bar{r}_0\bar{J}_{12}^+ - \frac{\partial^2}{\partial\bar{D}_{31}\partial\bar{D}_{31}}\bar{r}_0\bar{D}_{31} - \frac{\partial^2}{\partial\bar{D}_{31}\partial\bar{D}_{32}}(\bar{r}_0\bar{D}_{32}+\bar{s}_0\bar{D}_{31})\\
&-\frac{\partial^2}{\partial\bar{D}_{32}\partial\bar{J}_{13}^-}\bar{s}_0\bar{J}_{13}^- - \frac{\partial^2}{\partial\bar{D}_{32}\partial\bar{J}_{13}^+}\bar{s}_0\bar{J}_{13}^+ - \frac{\partial^2}{\partial\bar{D}_{32}\partial\bar{J}_{23}^-}\bar{s}_0\bar{J}_{23}^- - \frac{\partial^2}{\partial\bar{D}_{32}\partial\bar{J}_{23}^+}\bar{s}_0\bar{J}_{23}^+ - \frac{\partial^2}{\partial\bar{D}_{32}\partial\bar{J}_{12}^-}\bar{s}_0\bar{J}_{12}^-\\
&-\frac{\partial^2}{\partial\bar{D}_{32}\partial\bar{J}_{12}^+}\bar{s}_0\bar{J}_{12}^+ - \frac{\partial^2}{\partial\bar{D}_{32}\partial\bar{D}_{32}}\bar{s}_0\bar{D}_{32} - \frac{\partial^2}{\partial\bar{\alpha}\partial\bar{D}_{31}}\bar{g}_p\bar{J}_{13}^- + \frac{\partial^2}{\partial\bar{\alpha}\partial\bar{J}_{12}^+}\bar{g}_p\bar{J}_{23}^- + \frac{\partial^2}{\partial\bar{\alpha}\partial\bar{J}_{13}^+}\frac{\bar{g}_p}{3}(N+\bar{D}_{31}+\bar{D}_{32})\\
&-\frac{\partial^2}{\partial\bar{\alpha}^\dagger\partial\bar{D}_{31}}\bar{g}_p^*\bar{J}_{13}^+ + \frac{\partial^2}{\partial\bar{\alpha}^\dagger\partial\bar{J}_{12}^-}\bar{g}_p^*\bar{J}_{23}^+ + \frac{\partial^2}{\partial\bar{\alpha}^\dagger\partial\bar{J}_{13}^-}\frac{\bar{g}_p^*}{3}(N+\bar{D}_{31}+\bar{D}_{32}) - \frac{\partial^2}{\partial\bar{\beta}\partial\bar{D}_{32}}\bar{g}_r\bar{J}_{23}^- + \frac{\partial^2}{\partial\bar{\beta}\partial\bar{J}_{12}^-}\bar{g}_r\bar{J}_{13}^-\\
&+\frac{\partial^2}{\partial\bar{\beta}\partial\bar{J}_{23}^+}\frac{\bar{g}_r}{3}(N+\bar{D}_{31}+\bar{D}_{32}) - \frac{\partial^2}{\partial\bar{\beta}^\dagger\partial\bar{D}_{32}}\bar{g}_r^*\bar{J}_{23}^+ + \frac{\partial^2}{\partial\bar{\beta}^\dagger\partial\bar{J}_{12}^+}\bar{g}_r^*\bar{J}_{13}^+ + \frac{\partial^2}{\partial\bar{\beta}^\dagger\partial\bar{J}_{23}^-}\frac{\bar{g}_r^*}{3}(N+\bar{D}_{31}+\bar{D}_{32})\\
&+\frac{\partial^3}{\partial\bar{\alpha}\partial\bar{J}_{13}^+\partial\bar{J}_{13}^-}\frac{\bar{g}_p\bar{J}_{13}^-}{3} + \frac{\partial^3}{\partial\bar{\alpha}\partial\bar{J}_{13}^+\partial\bar{J}_{13}^+}\frac{\bar{g}_p\bar{J}_{13}^+}{3} + \frac{\partial^3}{\partial\bar{\alpha}\partial\bar{J}_{13}^+\partial\bar{J}_{23}^-}\frac{\bar{g}_p\bar{J}_{23}^-}{3}\\
&+\frac{\partial^3}{\partial\bar{\alpha}\partial\bar{J}_{13}^+\partial\bar{J}_{23}^+}\frac{\bar{g}_p\bar{J}_{23}^+}{3} + \frac{\partial^3}{\partial\bar{\alpha}\partial\bar{J}_{13}^+\partial\bar{J}_{12}^-}\frac{\bar{g}_p\bar{J}_{12}^-}{3} + \frac{\partial^3}{\partial\bar{\alpha}\partial\bar{J}_{13}^+\partial\bar{J}_{12}^+}\frac{\bar{g}_p\bar{J}_{12}^+}{3} + \frac{\partial^3}{\partial\bar{\alpha}\partial\bar{J}_{13}^+\partial\bar{D}_{31}}\frac{\bar{g}_p\bar{D}_{31}}{3}\\
&+\frac{\partial^3}{\partial\bar{\alpha}\partial\bar{J}_{13}^+\partial\bar{D}_{32}}\frac{\bar{g}_p\bar{D}_{32}}{3} + \frac{\partial^3}{\partial\bar{\alpha}^\dagger\partial\bar{J}_{13}^-\partial\bar{J}_{13}^-}\frac{\bar{g}_p^*\bar{J}_{13}^-}{3} + \frac{\partial^3}{\partial\bar{\alpha}^\dagger\partial\bar{J}_{13}^-\partial\bar{J}_{13}^+}\frac{\bar{g}_p^*\bar{J}_{13}^+}{3} + \frac{\partial^3}{\partial\bar{\alpha}^\dagger\partial\bar{J}_{13}^-\partial\bar{J}_{23}^-}\frac{\bar{g}_p^*\bar{J}_{23}^-}{3}\\
&+\frac{\partial^3}{\partial\bar{\alpha}^\dagger\partial\bar{J}_{13}^-\partial\bar{J}_{23}^+}\frac{\bar{g}_p^*\bar{J}_{23}^+}{3} + \frac{\partial^3}{\partial\bar{\alpha}^\dagger\partial\bar{J}_{13}^-\partial\bar{J}_{12}^-}\frac{\bar{g}_p^*\bar{J}_{12}^-}{3} + \frac{\partial^3}{\partial\bar{\alpha}^\dagger\partial\bar{J}_{13}^-\partial\bar{J}_{12}^+}\frac{\bar{g}_p^*\bar{J}_{12}^+}{3} + \frac{\partial^3}{\partial\bar{\alpha}^\dagger\partial\bar{J}_{13}^-\partial\bar{D}_{31}}\frac{\bar{g}_p^*\bar{D}_{31}}{3}\\
&+\frac{\partial^3}{\partial\bar{\alpha}^\dagger\partial\bar{J}_{13}^-\partial\bar{D}_{32}}\frac{\bar{g}_p^*\bar{D}_{32}}{3} + \frac{\partial^3}{\partial\bar{\beta}\partial\bar{J}_{23}^+\partial\bar{J}_{13}^-}\frac{\bar{g}_r\bar{J}_{13}^-}{3} + \frac{\partial^3}{\partial\bar{\beta}\partial\bar{J}_{23}^+\partial\bar{J}_{13}^+}\frac{\bar{g}_r\bar{J}_{13}^+}{3} + \frac{\partial^3}{\partial\bar{\beta}\partial\bar{J}_{23}^+\partial\bar{J}_{23}^-}\frac{\bar{g}_r\bar{J}_{23}^-}{3}\\
&+\frac{\partial^3}{\partial\bar{\beta}\partial\bar{J}_{23}^+\partial\bar{J}_{23}^+}\frac{\bar{g}_r\bar{J}_{23}^+}{3} + \frac{\partial^3}{\partial\bar{\beta}\partial\bar{J}_{23}^+\partial\bar{J}_{12}^-}\frac{\bar{g}_r\bar{J}_{12}^-}{3} + \frac{\partial^3}{\partial\bar{\beta}\partial\bar{J}_{23}^+\partial\bar{J}_{12}^+}\frac{\bar{g}_r\bar{J}_{12}^+}{3} + \frac{\partial^3}{\partial\bar{\beta}\partial\bar{J}_{23}^+\partial\bar{D}_{31}}\frac{\bar{g}_r\bar{D}_{31}}{3}\\
&+\frac{\partial^3}{\partial\bar{\beta}\partial\bar{J}_{23}^+\partial\bar{D}_{32}}\frac{\bar{g}_r\bar{D}_{32}}{3} + \frac{\partial^3}{\partial\bar{\beta}^\dagger\partial\bar{J}_{23}^-\partial\bar{J}_{13}^-}\frac{\bar{g}_r^*\bar{J}_{13}^-}{3} + \frac{\partial^3}{\partial\bar{\beta}^\dagger\partial\bar{J}_{23}^-\partial\bar{J}_{13}^+}\frac{\bar{g}_r^*\bar{J}_{13}^+}{3} + \frac{\partial^3}{\partial\bar{\beta}^\dagger\partial\bar{J}_{23}^-\partial\bar{J}_{23}^-}\frac{\bar{g}_r^*\bar{J}_{23}^-}{3}\\
&+\frac{\partial^3}{\partial\bar{\beta}^\dagger\partial\bar{J}_{23}^-\partial\bar{J}_{23}^+}\frac{\bar{g}_r^*\bar{J}_{23}^+}{3} + \frac{\partial^3}{\partial\bar{\beta}^\dagger\partial\bar{J}_{23}^-\partial\bar{J}_{12}^-}\frac{\bar{g}_r^*\bar{J}_{12}^-}{3} + \frac{\partial^3}{\partial\bar{\beta}^\dagger\partial\bar{J}_{23}^-\partial\bar{J}_{12}^+}\frac{\bar{g}_r^*\bar{J}_{12}^+}{3} + \frac{\partial^3}{\partial\bar{\beta}^\dagger\partial\bar{J}_{23}^-\partial\bar{D}_{31}}\frac{\bar{g}_r^*\bar{D}_{31}}{3}\\
&+\frac{\partial^3}{\partial\bar{\beta}^\dagger\partial\bar{J}_{23}^-\partial\bar{D}_{32}}\frac{\bar{g}_r^*\bar{D}_{32}}{3}\Bigg\}P(\mathbf{Z}),
\end{aligned}
\tag{A1c}
$$

where

$$\mathbf{Z}=(\bar{\alpha},\bar{\alpha}^\dagger,\bar{\beta},\bar{\beta}^\dagger,\bar{J}_{13}^+,\bar{J}_{13}^-,\bar{J}_{23}^+,\bar{J}_{23}^-,\bar{J}_{12}^+,\bar{J}_{12}^-,\bar{D}_{31},\bar{D}_{32}),$$

$$\bar{r}_0=\frac{1}{3}(\tilde{\Gamma}_1-\tilde{\Gamma}_2-2\bar{\gamma}_p-\bar{\gamma}_r),\qquad \bar{r}_1=\frac{1}{3}(-2\tilde{\Gamma}_1-\tilde{\Gamma}_2-2\bar{\gamma}_p-\bar{\gamma}_r),$$

$$\bar{r}_2=\frac{1}{3}(\tilde{\Gamma}_1+2\tilde{\Gamma}_2-2\bar{\gamma}_p-\bar{\gamma}_r),$$

$$\bar{s}_0=\frac{1}{3}(-\tilde{\Gamma}_1+\tilde{\Gamma}_2-\bar{\gamma}_p-2\bar{\gamma}_r),$$

$$\bar{s}_1=\frac{1}{3}(2\tilde{\Gamma}_1+\tilde{\Gamma}_2-\bar{\gamma}_p-2\bar{\gamma}_r),$$

$$\bar{s}_2=\frac{1}{3}(-\tilde{\Gamma}_1-2\tilde{\Gamma}_2-\bar{\gamma}_p-2\bar{\gamma}_r),$$

and

$$\bar{\gamma}_\perp^{12}=\frac{(\bar{\kappa}_1+\bar{\kappa}_2+\bar{\Gamma}_1+\bar{\Gamma}_2)}{2},$$

$$\bar{\gamma}_\perp^{13}=\frac{(\bar{\kappa}_1+\bar{\kappa}_3+\bar{\Gamma}_1+\bar{\gamma}_p+\bar{\gamma}_r)}{2},$$

$$\bar{\gamma}_\perp^{23}=\frac{(\bar{\kappa}_2+\bar{\kappa}_3+\bar{\Gamma}_2+\bar{\gamma}_p+\bar{\gamma}_r)}{2}.$$

APPENDIX B

The noise correlation terms for the noises appearing in Eqs. (31)–(42) are as follows. These correspond to the second-order terms of the FPE given in Appendix A, but have undergone the scaling and transformation to a rotating frame as described in the text:

$$\langle\Gamma_\alpha(t)\Gamma_{D_{31}}(t')\rangle=-g_pJ_{13}^-\delta(t-t'),$$

$$\langle\Gamma_{\alpha^\dagger}(t)\Gamma_{D_{31}}(t')\rangle=-g_p^*J_{13}^+\delta(t-t'),$$

$$\langle\Gamma_\alpha(t)\Gamma_{J_{12}^+}(t')\rangle=g_pJ_{23}^-\delta(t-t'),$$

$$\langle\Gamma_{\alpha^\dagger}(t)\Gamma_{J_{12}^-}(t')\rangle=g_p^*J_{23}^+\delta(t-t'),$$

$$\langle\Gamma_\alpha(t)\Gamma_{J_{13}^+}(t')\rangle=\frac{g_p}{3}(1+D_{31}+D_{32})\,\delta(t-t'),$$

$$\langle\Gamma_{\alpha^\dagger}(t)\Gamma_{J_{13}^-}(t')\rangle=\frac{g_p^*}{3}(1+D_{31}+D_{32})\,\delta(t-t'),$$

$$\langle\Gamma_\beta(t)\Gamma_{D_{32}}(t')\rangle=-g_rJ_{23}^-\delta(t-t'),$$

$$\langle\Gamma_{\beta^\dagger}(t)\Gamma_{D_{32}}(t')\rangle=-g_r^*J_{23}^+\delta(t-t'),$$

$$\langle\Gamma_\beta(t)\Gamma_{J_{23}^+}(t')\rangle=\frac{g_r}{3}(1+D_{31}+D_{32})\,\delta(t-t'),$$

$$\langle\Gamma_{\beta^\dagger}(t)\Gamma_{J_{23}^-}(t')\rangle=\frac{g_r^*}{3}(1+D_{31}+D_{32})\,\delta(t-t'),$$

$$\langle\Gamma_\beta(t)\Gamma_{J_{12}^-}(t')\rangle=g_rJ_{13}^-\delta(t-t'),$$

$$\langle\Gamma_{\beta^\dagger}(t)\Gamma_{J_{12}^+}(t')\rangle=g_r^*J_{13}^+\delta(t-t'),$$

$$\langle\Gamma_{J_{12}^+}(t)\Gamma_{D_{31}}(t')\rangle=-r_0J_{12}^+\delta(t-t'),$$

$$\langle\Gamma_{J_{12}^+}(t)\Gamma_{D_{32}}(t')\rangle=-s_0J_{12}^+\delta(t-t'),$$

$$\langle\Gamma_{J_{13}^+}(t)\Gamma_{D_{31}}(t')\rangle=-r_0J_{13}^+\delta(t-t'),$$

$$\langle\Gamma_{J_{13}^+}(t)\Gamma_{D_{32}}(t')\rangle=-s_0J_{13}^+\delta(t-t'),$$

$$\langle\Gamma_{J_{23}^+}(t)\Gamma_{D_{31}}(t')\rangle=-r_0J_{23}^+\delta(t-t'),$$

$$\langle\Gamma_{J_{23}^+}(t)\Gamma_{D_{32}}(t')\rangle=-s_0J_{23}^+\delta(t-t'),$$

$$\langle\Gamma_{D_{31}}(t)\Gamma_{D_{31}}(t')\rangle=-2r_0D_{31}\delta(t-t'),$$

$$\langle\Gamma_{D_{31}}(t)\Gamma_{D_{32}}(t')\rangle=-(r_0D_{32}+s_0D_{31})\,\delta(t-t'),$$

$$\langle\Gamma_{D_{31}}(t)\Gamma_{J_{12}^-}(t')\rangle=-r_0J_{12}^-\delta(t-t'),$$

$$\langle\Gamma_{D_{31}}(t)\Gamma_{J_{13}^-}(t')\rangle=-r_0J_{13}^-\delta(t-t'),$$

$$\langle\Gamma_{D_{31}}(t)\Gamma_{J_{23}^-}(t')\rangle=-r_0J_{23}^-\delta(t-t'),$$

$$\langle\Gamma_{D_{32}}(t)\Gamma_{D_{32}}(t')\rangle=-2s_0D_{32}\delta(t-t'),$$

$$\langle\Gamma_{D_{32}}(t)\Gamma_{J_{12}^-}(t')\rangle=-s_0J_{12}^-\delta(t-t'),$$

$$\langle\Gamma_{D_{32}}(t)\Gamma_{J_{13}^-}(t')\rangle=-s_0J_{13}^-\delta(t-t'),$$

$$\langle\Gamma_{D_{32}}(t)\Gamma_{J_{23}^-}(t')\rangle=-s_0J_{23}^-\delta(t-t').$$

APPENDIX C

The fifteen equations obtained using the definitions (43) are as follows. These equations are independent of the Raman frequency:

$$\dot{U}_1=-\kappa U_1+g_rU_8+\frac{\Gamma_{U_1}}{\sqrt{N}},$$

$$\dot{U}_2=-\frac{\kappa}{2}U_2+\phi_1U_3+g_pU_4-i(\varepsilon-\varepsilon^*)+\frac{\Gamma_{U_2}}{\sqrt{N}},$$

$$\dot{U}_3=-\frac{\kappa}{2}U_3-\phi_1U_2+g_pU_7+(\varepsilon+\varepsilon^*)+\frac{\Gamma_{U_3}}{\sqrt{N}},$$

$$\dot{U}_4=-\gamma_\perp^{13}U_4+\Delta U_7-g_rU_6+g_pU_{10}U_2+\frac{\Gamma_{U_4}}{\sqrt{N}},$$

$$\dot{U}_5=-\left(\frac{\kappa}{2}+\gamma_\perp^{23}\right)U_5+(\phi_2-\Delta)U_8+\frac{g_p}{2}(U_9U_2-U_6U_3)+\frac{\Gamma_{U_5}}{\sqrt{N}},$$

$$\dot{U}_6=-\left(\frac{\kappa}{2}+1\right)U_6+\phi_2U_9+\frac{g_p}{2}(U_8U_2+U_5U_3)+g_r(U_4U_1+U_{13})+\frac{\Gamma_{U_6}}{\sqrt{N}},$$

$$\dot{U}_7=-\gamma_\perp^{13}U_7-\Delta U_4-g_rU_9+g_pU_{10}U_3+\frac{\Gamma_{U_7}}{\sqrt{N}},$$

$$\dot{U}_8=-\left(\frac{\kappa}{2}+\gamma_\perp^{23}\right)U_8-(\phi_2-\Delta)U_5-\frac{g_p}{2}(U_6U_2+U_9U_3)+2g_r(U_{11}U_1+U_{12})+\frac{\Gamma_{U_8}}{\sqrt{N}},$$

$$\dot{U}_9=-\left(\frac{\kappa}{2}+1\right)U_9-\phi_2U_6+\frac{g_p}{2}(U_8U_3-U_5U_2)+g_r(U_7U_1+U_{14})+\frac{\Gamma_{U_9}}{\sqrt{N}},$$

$$\dot{U}_{10}=-g_p(U_4U_2+U_7U_3)-g_rU_8+r_0+r_1U_{10}+r_2U_{11}+\frac{\Gamma_{U_{10}}}{\sqrt{N}},$$

$$\dot{U}_{11}=-\frac{g_p}{2}(U_4U_2+U_7U_3)-2g_rU_8+s_0+s_1U_{10}+s_2U_{11}+\frac{\Gamma_{U_{11}}}{\sqrt{N}},$$

$$\dot{U}_{12}=-2\gamma_\perp^{23}U_{12}-\frac{g_p}{2}(U_{14}U_3+U_{13}U_2)+g_rU_{11}U_8+\frac{\Gamma_{U_{12}}}{\sqrt{N}},$$

$$\dot{U}_{13}=-(\gamma_\perp^{23}+1)U_{13}+\Delta U_{14}+g_p(U_{12}-U_{15})U_2+\frac{g_r}{2}(U_8U_4-U_5U_7)+g_rU_{11}U_6+\frac{\Gamma_{U_{13}}}{\sqrt{N}},$$

$$\dot{U}_{14}=-(\gamma_\perp^{23}+1)U_{14}-\Delta U_{13}+g_p(U_{12}-U_{15})U_3+\frac{g_r}{2}(U_5U_4+U_8U_7)+g_rU_{11}U_9+\frac{\Gamma_{U_{14}}}{\sqrt{N}},$$

$$\dot{U}_{15}=-2U_{15}+\frac{g_p}{2}(U_{14}U_3+U_{13}U_2)+\frac{g_r}{2}(U_6U_4+U_9U_7)+\frac{\Gamma_{U_{15}}}{\sqrt{N}},$$

where

$$\Gamma_{U_1}=\Gamma_{\beta^\dagger}\beta+\Gamma_\beta\beta^\dagger,$$

$$\Gamma_{U_2}=-i\Gamma_\alpha+i\Gamma_{\alpha^\dagger},$$

$$\Gamma_{U_3}=\Gamma_\alpha+\Gamma_{\alpha^\dagger},$$

$$\Gamma_{U_4}=-i\Gamma_{J_{13}^-}+i\Gamma_{J_{13}^+},$$

$$\Gamma_{U_5}=-iJ_{23}^+\Gamma_\beta+iJ_{23}^-\Gamma_{\beta^\dagger}-i\beta\Gamma_{J_{23}^+}+i\beta^\dagger\Gamma_{J_{23}^-},$$

$$\Gamma_{U_6}=-iJ_{12}^-\Gamma_\beta+iJ_{12}^+\Gamma_{\beta^\dagger}-i\beta\Gamma_{J_{12}^-}+i\beta^\dagger\Gamma_{J_{12}^+},$$

$$\Gamma_{U_7}=\Gamma_{J_{13}^-}+\Gamma_{J_{13}^+},$$

$$\Gamma_{U_8}=J_{23}^+\Gamma_\beta+J_{23}^-\Gamma_{\beta^\dagger}+\beta\Gamma_{J_{23}^+}+\beta^\dagger\Gamma_{J_{23}^-},$$

$$\Gamma_{U_9}=J_{12}^-\Gamma_\beta+J_{12}^+\Gamma_{\beta^\dagger}+\beta\Gamma_{J_{12}^-}+\beta^\dagger\Gamma_{J_{12}^+},$$

$$\Gamma_{U_{10}}=\Gamma_{D_{31}},$$

$$\Gamma_{U_{11}}=\Gamma_{D_{32}},$$

$$\Gamma_{U_{12}}=\Gamma_{J_{23}^+}J_{23}^-+\Gamma_{J_{23}^-}J_{23}^+,$$

$$\Gamma_{U_{13}}=-iJ_{23}^-\Gamma_{J_{12}^-}+iJ_{23}^+\Gamma_{J_{12}^+}-iJ_{12}^-\Gamma_{J_{23}^-}+iJ_{12}^+\Gamma_{J_{23}^+},$$

$$\Gamma_{U_{14}}=J_{23}^-\Gamma_{J_{12}^-}+J_{23}^+\Gamma_{J_{12}^+}+J_{12}^-\Gamma_{J_{23}^-}+J_{12}^+\Gamma_{J_{23}^+},$$

$$\Gamma_{U_{15}}=\Gamma_{J_{12}^+}J_{12}^-+\Gamma_{J_{12}^-}J_{12}^+.$$

The Γ_{U_i} cannot be expressed in terms of the U_i, however the noise correlations $\langle\Gamma_{U_i}(t)\Gamma_{U_j}(t')\rangle$ which are used in calculating the spectrum can, by using the correlations in Appendix B, and the definitions in Eq. (43).

[1] N. Bloembergen, Am. J. Phys. **37**, 989 (1967).

[2] M.G. Raymer and J. Mostowski, Phys. Rev. A **24**, 1980 (1981).

[3] B.J. Herman, J.H. Eberly, and M.G. Raymer, Phys. Rev. A **39**, 3447 (1989).

[4] R.G. Harrison and D.J. Biswas, Phys. Rev. Lett. **55**, 63 (1985).

[5] R.G. Harrison, W. Lu, and P.K. Gupta, Phys. Rev. Lett. **63**, 1372 (1989).

[6] W. Lu and R.G. Harrison, Phys. Rev. A **41**, 6563 (1990).

[7] W. Lu and R.G. Harrison, Phys. Rev. A **43**, 6358 (1991).

[8] R. Corbalán, J. Cortit, and F. Prati, Phys. Rev. A **53**, 481 (1996).
[9] I.A. Walmsley and M.G. Raymer, Phys. Rev. Lett. **50**, 962 (1983).
[10] D.C. MacPherson, R.C. Swanson, and J.L. Carlsten, Phys. Rev. A **39**, 3487 (1989).
[11] M.G. Raymer, Z.W. Li, and I.A. Walmsley, Phys. Rev. Lett. **63**, 1586 (1989).
[12] J.C. Englund and C.M. Bowden, Phys. Rev. A **42**, 2870 (1990).
[13] K.M. Gheri and D.F. Walls, Phys. Rev. A **45**, 6675 (1992).
[14] H. Ritsch, M.A.M. Marte, and P. Zoller, Europhys. Lett. **19**, 7 (1992).
[15] K.M. Gheri and D.F. Walls, Phys. Rev. Lett. **68**, 3428 (1992).
[16] A.S. Manka *et al.*, Opt. Commun. **94**, 174 (1992).
[17] H. Ritsch and M.A.M. Marte, Phys. Rev. A **47**, 2354 (1993).
[18] K.J. Schernthanner and H. Ritsch, Phys. Rev. A **49**, 4126 (1994).
[19] X.-W. Xia, W.J. Sandle, R.J. Ballagh, and D.M. Warrington, Phys. Rev. A **53**, 2641 (1996).
[20] H. Haken, H. Risken, and W. Weidlich, Z. Phys. **206**, 355 (1967).
[21] P.D. Drummond and D.F. Walls, Phys. Rev. A **23**, 2563 (1981).
[22] A.M. Smith and C.W. Gardiner, Phys. Rev. A **38**, 4073 (1988).
[23] C.W. Gardiner, *Quantum Noise* (Springer-Verlag, Heidelberg, 1991).
[24] Our equations can then be shown to agree with those of Xia *et al.* if we make the correspondences $\gamma_{\perp}^{13} \equiv \kappa_1^X$, $\gamma_{\perp}^{23} \equiv \kappa_2^X$, $\kappa/2 \equiv \kappa^X$, $\alpha \equiv -i\alpha^X/g_p^*$, $\beta \equiv -i\beta^X g_r^*$, $g_p = \sqrt{g_1}$, $g_r = \sqrt{g_2}$, and $\varepsilon \equiv -i\kappa\alpha_s/2\sqrt{g_1}$, where Xia's variables appear on the right-hand side of these definitions, and we have denoted them with the superscript X where necessary to avoid ambiguity.
[25] X.-W. Xia, Ph.D. thesis, University of Otago, New Zealand (1993).
[26] In the Ito calculus $d(ab) = a(db) + (da)b + (da)(db)$. The final term is the Ito contribution. It does not appear if ordinary calculus rules are applied.
[27] Available from directory `pub/doedel/auto` at ftp.cs.concordia.ca
[28] G.P. Agrawal and H.J. Carmichael, Phys. Rev. A **19**, 2074 (1979).